文章编号：1001-9014(2022)06-1022-08

DOI:10.11972/j.issn.1001-9014.2022.06.011

Regulation on microstructural and optical properties of Sb_2Te_3 films induced by titanium doping

LIAO Yuan-Jie[1], LI Yao-Peng[1], SONG Xiao-Xiao[1], ZHANG Xin-Tong[1], ZHANG Shu-Bo[1], ZHANG Teng-Fei[1], LUY Meng-Qi[1], LIU Zhen[1], ZOU Yi-Yun[1], ZHANG Ye[1], HU Er-Tao[2*], LI Jing[1,3*]

(1. Department of Optical Science and Engineering, Shanghai Ultra-Precision Optical Manufacturing Engineering Center, Fudan University, Shanghai 200438, China;
2. College of Electronic and Optical Engineering, Nanjing University of Posts and Telecommunications, Nanjing 210023, China;
3. Key Laboratory of Micro and Nano Photonic Structures (Ministry of Education), Fudan University, Shanghai 200433, China)

Abstract: In this work, the doping effects of Ti on the structural, linear optical properties and nonlinear absorption of Sb_2Te_3 thin films were systematically studied. A magnetron sputtering system and an annealing furnace are employed to prepare the crystalline Sb_2Te_3 samples with different doping concentrations of Ti. The X-ray photoelectron spectroscopy analysis confirmed that the Ti element exists in the Sb_2Te_3 films is in the form of $TiTe_2$, in which the chemical state of Ti^{4+} arises. For linear optical properties, the results indicate that the Ti dopant can improve the transmittance of the Sb_2Te_3 films, when a wide working wavelength is used in the nonlinear devices. The optical band gap decreases from 1.32 eV to 1.25 eV for the Ti-doped Sb_2Te_3 films, which is dependent on the reduction of carriers according to the Burstein-Moss theory. An open-aperture Z-scan system is set up to determine the nonlinear saturated absorption of the film samples, which is excited by an 800 nm femtosecond laser at a power of 132 GW/cm^2. Moreover, the adjustable behavior caused by Ti doping could be attributed to the competition between the decrease in the optical band gap and the inhibition of the crystallization. Additionally, it is interesting to find that the Ti doping improves the laser damage threshold of the Sb_2Te_3 thin films from 188.6 to 265.5 GW/cm^2. In general, the Ti-doped Sb_2Te_3 thin films have wide-ranging application possibilities for the field of nonlinear optical devices.

Key words: Ti-dopant, Sb_2Te_3 thin film, optical band gap, saturable absorption, open-aperture Z-scan

Ti掺杂对Sb_2Te_3薄膜的结构及光学性质的调控

廖袁杰[1], 李耀鹏[1], 宋晓晓[1], 张欣彤[1], 张书博[1], 张腾飞[1], 吕孟奇[1], 刘 镇[1], 邹意蕴[1], 张 野[1], 胡二涛[2*], 李 晶[1,3*]

(1. 复旦大学 光科学与工程系上海超精密光学制造工程技术研究中心,上海 200438;
2. 南京邮电大学 电子与光学工程学院&微电子学院,江苏 南京 210023;
3. 复旦大学 微纳光子结构教育部重点实验室,上海 200433)

摘要:对Sb_2Te_3薄膜的结构、线性光学及非线性吸收性质的Ti掺杂影响进行了系统性探究。利用磁控溅射和高温退火手段制备了不同Ti掺杂浓度的晶态Sb_2Te_3薄膜。X射线光电子能谱分析显示Sb_2Te_3薄膜中的Ti元素以Ti^{4+}化学态以$TiTe_2$的形式存在。线性光学性质结果表明,在保持非线性器件中宽工作波长特性的同时,Ti掺杂可以提高Sb_2Te_3薄膜的透射率,并降低光学带隙从1.32 eV至1.25 eV,根据Burstein-Moss理论,这取决于

Received date: 2022-06-16, **revised date**: 2022-09-02 **收稿日期**:2022-06-16,**修回日期**:2022-09-02

Foundation items: Supported by National Natural Science Foundation of China (60578047, 61427815), Natural Science Foundation of Shanghai (17ZR1402200, 13ZR1402600)

Biography: LIAO Yuan-Jie (1997-), male, Shanghai, China, Master. Research area involves optical properties of chalcogenide thin films
E-mail: 19210720009@fudan.edu.cn

* **Corresponding author**: E-mail: iamethu@njupt.edu.cn, lijing@fudan.edu.cn

载流子的减少。利用自主搭建的开孔Z扫描系统,测试了薄膜样品在132 GW/cm²强度下800 nm飞秒激光激发的非线性吸收性质,结果显示的Ti掺杂引起的饱和吸收可调谐行为可归因于光学带隙减小与晶化抑制的竞争效应。此外,Ti掺杂将Sb_2Te_3薄膜的激光损伤阈值从188.6 GW/cm²提高到了265.5 GW/cm²。总而言之,Ti掺杂Sb_2Te_3薄膜在非线性光学器件领域具有广泛的应用前景。

关　键　词:钛掺杂;碲化锑薄膜;光学带隙;饱和吸收;开孔Z扫描

中图分类号:O43　　**文献标识码**:A

Introduction

Chalcogenide thin films, due to their excellent optical and electrical properties, are widely used in the fields of phase change random-access memory (PRAM), solar cells, nonlinear optical absorption (NOA) devices and so on [1-3]. In particular, these types of materials, which have become a hot topic recently owing to their large nonlinear absorption coefficient, are regarded as efficient nonlinear materials with high potential for areas such as mode-locking and optical limiting [4]. Among them, the transition metal chalcogenides including MoS_2, $MoSe_2$ and $MoTe_2$ have been found to have the saturated absorption effect in recent years [5]. Others, such as CdTe, ZnS and ZnSe, exhibit the inverse saturable absorption effect, that is, the two-photon absorption effect of the light attenuation caused by the simultaneous absorption of two photons by the material [6]. To better adapt them to the practical application, a few methods have been researched in the past few years to regulate their NOA properties, which include employing a phase-change [7], modifying the film thickness [8], photodarkening [9] and designing a multilayer structure [10] etc. Among them, doping with Ti is an effective method. For example, Ti is found to have significant effects when regulating the structural and optical properties of the chalcogenide thin film, particularly in the fields of phase memory and lasers [11-12].

As a member of the binary chalcogenides, Sb_2Te_3 is a p-type semiconductor that contains a narrow direct band [13]. Considerable efforts have been devoted to its resistance-switching behaviors [14], phase change [15], thermoelectric [16] and excellent optical properties [17]. In particular, the widespread application of graphene with nonlinear saturable absorption characteristics [18], Bi_2Te_3, Bi_2Se_3 and Sb_2Te_3 with topological insulating properties[19] in chalcogenide compounds exhibit their nonlinear saturated absorptions [20-22], which have promise as a kind of potential materials in nonlinear modulator devices for an ultrafast laser. There are also many doping studies on Sb_2Te_3, although most of them focus on the effects on its crystalline, electrical and thermal conductivity [23-24]. Importantly, in the study of the thermoelectric properties of Ti-doped Sb_2Te_3 samples, interesting phenomenon relating to a decrease in the carrier concentration was found[25]. There is no such effects arise in other dopants such as Cr [26]. According to the Moss-Burstein theorem, the optical band gap is directly related to the carrier concentration [27]. By regulating of Ti doping concentration, it should also have a large impact on the regulation of nonlinear absorption, due to its effect on the optical band gap of thin film samples.

Based on the factors provided above, titanium as the dopant is chosen. Through analysis of the experimental data, and a theoretical discussion, we concentrate on the regulation effects of the Ti dopant in relation to optical properties of the Sb_2Te_3 thin films. Furthermore, the mouldability of transmittance, optical band gap and nonlinear absorption coefficient of the film samples by Ti dopants is thoroughly analyzed. It is shown that the Ti-doped Sb_2Te_3 films hold great promise for nonlinear optical applications.

1 Experiments

1.1 Sample preparation

The magnetron sputtering system (EBAS, Infovion, South Korea) is used to prepare film samples in the study. Ti-doped Sb_2Te_3 thin films were deposited on fused quartz substrates and Si (100) by radio-frequency (RF) co-sputtering mode using Sb_2Te_3 and Ti targets with a purity of 99.99%. Each substrate is treated respectively with alcohol, acetone, and deionized water in an ultrasonic cleaning equipment, then blown-dried using nitrogen. The working pressure was controlled at 2 mTorr and the chamber temperature was at room temperature. The sputtering power of the Sb_2Te_3 target magnetron was set to 80W constant, and sputtering time of all samples was fixed at 125 s. In order to prepare Ti-doped Sb_2Te_3 samples at different concentrations, the sputtering powers of Ti target magnetron were set up to 0 W, 30 W, 40 W and 50 W respectively, shown in Table 1. After depositions, to obtain crystalline Ti-doped Sb_2Te_3 films, a set of samples was annealed at 573 K for 30 min in a flowing nitrogen atmosphere. Based on preliminary experiments and previous experimental experiences, it can be ensured that the film samples have had sufficient time to crystallize at the setup temperature.

Table 1　The sputtering power and time of Ti-doped Sb_2Te_3 thin films

表1　Ti掺杂Sb2Te3薄膜的溅射功率及时间

Sample Number	Sb_2Te_3 Power /W	Ti Power /W	Sputtering Time/s
S1	80	0	125
S2	80	30	125
S3	80	40	125
S4	80	50	125

1.2 Characterization methods

For the overall morphology and thickness of the samples, the scanning electron microscopy (SEM) (Sigma

300, Zeiss, Germany) mapping scan are employed and the resolution is 1.0 nm @ 15 kV. Further, energy dispersive X-ray spectroscopy (EDS) (Smartedx, Zeiss, Germany) elemental analysis is performed to establish the element composition of the samples, in with particular attention to the Ti doping content.

For the material itself, the crystal structure of the samples is carried out by X-ray di ff raction (XRD) (Bruker D8 ADVANCE, Karlsruhe, Germany) with the Cu-Kα (1.540 56 Å) radiation. The 2θ angle is in the range of $10^\circ \sim 60^\circ$ with a step of 0.02°. The valence states of its constituent elements are measured by X-ray photoelectron spectroscopy (XPS) (K-Alpha, Thermo Scientific, USA).

For linear optical properties, the transmission spectroscopic characteristics are determined by spectrophotometer (UV - VIS - NIR, Shimadzu, Japan). Moreover, the spectroscopic ellipsometry (SE) [28], is used and the linear optical constants (include the refractive index n and extinction coefficient κ) are fitted by software FilmWizard® in the wavelength range of 350~850 nm.

For nonlinear absorption properties, the open-aperture (OA) mode Z-scan system had been built which introduced in our previous work [3]. A Ti-sapphire laser (Spectra Physics, USA) is used to excite the samples with 800 nm wavelength and 100 fs pulse duration. In the experiment, the sample is moved near the laser focus by a focusing lens (300 mm) and a stepping motor. By measurement, the Rayleigh length (Z_0) is 4 mm and the focal beam radius (ω) is 32 μm at the focal point that is much larger than the film thickness. This condition is found to be critical in the Z-scan theory [29].

2 Results and discussions

2.1 Film thickness and composition

The thickness and the Ti atomic ratios of the Ti-doped Sb_2Te_3 thin films, which is measured by SEM and EDS, are listed in Table 2. It is feasible to increase the doping concentration of the samples with increasing the sputtering power of Ti target magnetron. The atomic ratios of Ti are 0%, 4.00%, 5.37% and 6.64% of the S1-S4 samples, respectively.

2.2 crystalline structure and chemical state

The XRD patterns of the annealed samples (S1-S4) are shown in Fig. 1. After removing the background intensity, the images show four diffraction peaks, indicating that the samples have been in a distinct crystalline state. On a comparison with the standard diffraction PDF card, these four diffraction peaks including (006), (009), (0015) and (0018) are correspond to the R3m rhombohedral structure, in which the lattice constants are $a = b = 4.262$ Å and $c = 30.45$ Å (JCPDS No: 015-0874). The same structure has been reported in some earlier research [30] about Sb_2Te_3, it also states that Ti is completely enclosed within the crystalline and acts as a doping element.

Table 2 The thickness and the Ti atomic ratios of Ti-doped Sb_2Te_3 thin films
表2 Ti掺杂Sb_2Te_3薄膜的厚度及Ti原子比例

Sample Number	Ti Target Power /W	Ti (Atomic %)	Thickness/nm
S1	0	0	61.42
S2	30	4.00	62.29
S3	40	5.37	65.87
S4	50	6.64	67.03

Moreover, considering the simultaneous effects of crystal size and lattice strain on the XRD diffraction peak broadening, the lattice parameters have been calculated by using the Williamson-Hall relation (1) [31] as follows.

$$B\cos\theta = \varepsilon(4\sin\theta) + \frac{k\lambda}{D} \quad , \quad (1)$$

where λ is the wavelength of the X-ray radiation (1.54056 Å), B is the FWHM of the diffraction peak, and θ is the angle for the Bragg diff raction. The values of the average grain size D and the lattice strain $\boldsymbol{\varepsilon}$ are obtained from the intercept and slope. As shown in Table 3, the average grain size in the film decreases with the increase of Ti doping concentration, but the lattice strain and dislocation density increase, indicating effective inhibition of crystallization. Similar findings are found in studies on the phase change of the Ti-doped Sb_2Te_3 thin films [32]. This should be due to Ti element doping making certain elements in the Sb_2Te_3 structure be replaced to form a new bonding structure. This type of phase change material shows a nucleation-dominated behavior. For the same volume, more nucleation centers mean smaller grain sizes [33]. While the stress, along with the defects on the grain boundaries, also inhibits the grain growth.

X-ray photoelectron spectroscopy (XPS) is applied to characterize the chemical valence and the bonding modes of Ti doped Sb_2Te_3 samples. The XPS test uses Al Kα x-rays (1486.6 eV) to scan the binding energy (BE) spectrum and the concerned peaks of the film samples. Scanning spectra were recorded at energy steps of 1 eV, and the peak regions were recorded at energy steps of 0.1 eV. In order to correct the binding energy of the elements, the raw data from XPS spectrometer were calibrated according to the standard value of C_{1s} 284.6 eV recom-

Table 3 Effect of Ti doping on the structural parameters of the Ti-doped Sb_2Te_3 films
表3 Ti掺杂Sb_2Te_3薄膜的结构参数影响

Sample	Ti (Atomic %)	Crystallite Size /nm	Lattice Strain (10^{-3})	Dislocation Density ($1/D^2$ 10^{-4} nm^{-2})
S1	0	37.34	6.07	7.17
S2	4.00	31.39	7.22	10.14
S3	5.37	25.40	8.93	15.49
S4	6.64	20.58	11.02	23.59

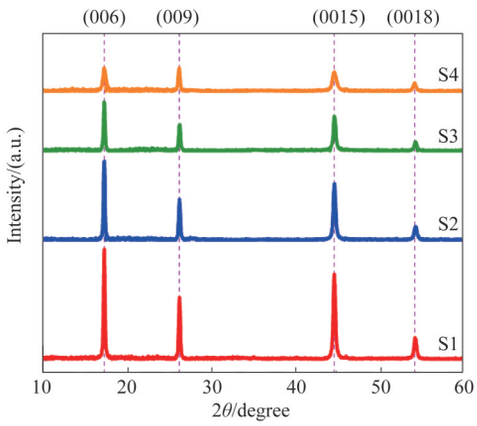

Fig. 1　XRD patterns of the Ti-doped Sb_2Te_3 thin films
图 1　Ti掺杂Sb_2Te_3薄膜的X射线衍射图

mended by the instrument, and then performed peak fittings. As plotted in Figure 2a, the energies of two high intensity peaks are 529. 1 eV and 538. 5 eV, corresponding to the $3d_{5/2}$ and $3d_{3/2}$ of Sb, respectively. Similarly, two intense peaks are found at 572. 6 eV and 583. 0 eV, matching with the $3d_{5/2}$ and $3d_{3/2}$ of Te, respectively, in Figure 2b. And there is a small decrease in the binding energies of Sb and Te after doping with Ti, due to the smaller electronegativity of Ti dopant. An interesting found is that, as shown in Figure 2c, unlike the performances of Ti dopant in other compounds, the Ti doped Sb_2Te_3 samples do appear as two obviously independent peaks at about 459. 1 eV and 464. 8 eV, corresponding to the Ti $2p_{3/2}$ and Ti $2p_{1/2}$, respectively. By comparing this with other energy spectra involving Ti (2+, 3+, 4+) dopant, this result implies that the Ti dopant behaves as Ti^{4+} valence state, as indicated to form $TiTe_2$ while Ti is doped into the Sb_2Te_3 thin films at a certain doping concentration. This result support our previous research conclusion that a certain concentration of titanium is doped in $Ge_2Sb_2Te_5$ [34], apparently the components of GeTe and Sb_2Te_3 in the pseudo-ternary $Ge_2Sb_2Te_5$ makes the doping effect more complicated. It proves that the regulatory effect on Sb_2Te_3 with the titanium doping directly is more advantageous. This is the original intention of this study expected to effectively regulate the optical properties of Sb_2Te_3 films through titanium doping.

According to the Krebs model [34], the Ti atom that occupies the Sb position provides three electrons that participate in the bonding with the Te atoms, and the extra electrons are released. In the Sb_2Te_3 lattice structure, the composition of Ti atoms can be described as follows.

$$Sb_2Te_3 + 2Ti \rightarrow 2Sb + Ti_2^{sb}Te_3 + 2e \quad . \quad (2)$$

This experimental result further demonstrates the replacement model, showing that the increased titanium content and bonding to Te element replacing Sb element leads to a reduction in the crystalline size. In p-type semiconductors, the electrons released by this bonding mechanism will combine with the holes, which results in a reduction in the carrier concentration, this is also consistent with previous studies on reflectance and the galvanomagnetic of Ti-doped Sb_2Te_3 [27, 35].

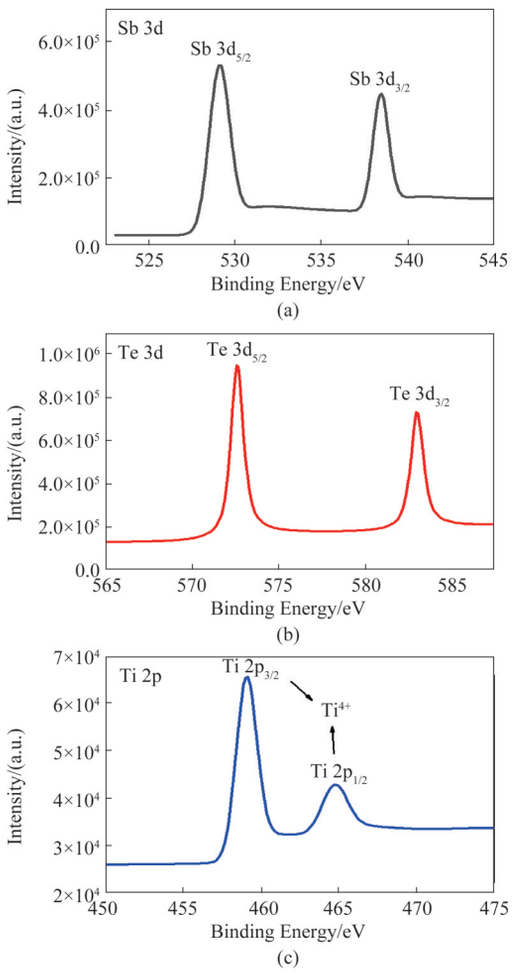

Fig. 2　XPS spectra of the Ti-doped Sb_2Te_3 films (a) Sb 3d, (b) Te 3d, (c) Ti 2p
图 2　Ti掺杂Sb2Te3薄膜的X射线光电子能谱图 (a) Sb 3d, (b) Te 3d, (c) Ti 2p

2. 3　Linear optical properties

The optical transmission spectrum, with an infrared range of 750~1 600 nm applied to the Ti-doped Sb_2Te_3 thin films, is presented in Fig. 3 (a). The spectral curves of the samples are relatively flat with varying different titanium doping ratios. It indicates that a broad spectral working bandwidth can be obtained for the sample films doped in this way. For example, as a saturated absorber, there is no significant change in the linear transmittance in the wavelength range around 1 550 nm for the Er-doped lasers [10]. Specifically, the transmittance of the films increases with the increasing of Ti dopant, it can maintain the excellent optical characteristics in the wide working bandwidth controlled by Ti doping at the low concentration. Furthermore, the elliptic polarization parameters were obtained using the SE experiments at the three incident angles of 65, 70, and 75. Based on the Lorentz oscillator model, the fitting error was controlled within 0. 01 using FilmWizard® software. The refractive index curves are shown in Fig. 3(b).

To determine the absorption properties of the samples, various formulas can be used that intuitively reflect

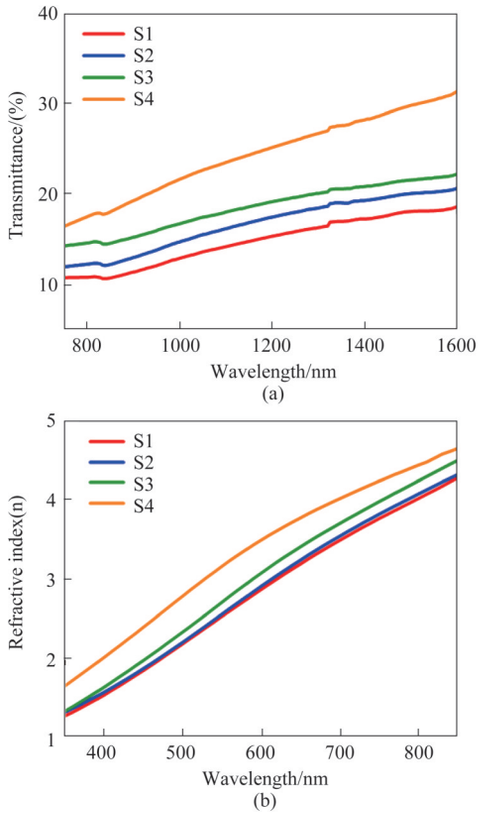

Fig. 3 (a) Transmittance and (b) refractive index curves of the Ti-doped Sb_2Te_3 thin films
图3 Ti掺杂Sb_2Te_3薄膜的(a)透射谱和(b)折射率曲线

the extinction coefficient, κ, and the optical band gap, E_g. The linear absorption coefficient, α, is a critical variable, which can be calculated by the following Eq. 3.

$$\alpha = \frac{4\pi\kappa}{\lambda} \quad . \quad (3)$$

According to Tauc's theory [36], the optical band gap can be estimated by using the following Eq. 4,

$$(\alpha h\nu) = A\left(h\nu - E_g\right)^n \quad , \quad (4)$$

where $h\nu$ is the photon energy, and A is a constant determined from the effective mass. The exponent n depends on the electronic transition properties of materials. Depending on their types, the n have different values, such as 1/2, 2, 3/2 and 3, corresponding to direct allowed, indirect allowed, direct forbidden and indirect forbidden band gaps, respectively[37]. For the Sb_2Te_3 thin films with a direct allowed narrow band gap [38], n value is the constant of 1/2. It can also be seen, from the above equation, that the optical band gap E_g can be obtained from the x-axis intercept value of the linear part of the curve, that is, when a value of $\alpha h\nu$ is set to 0. As a very useful parameter for determining the degree of disorder, the Tauc parameter A, which contains valence and conduction band states, can be obtained from the slope [39]. With the increase of the Ti doping concentration, the relative values of A2 corresponding to the slopes of the S1-S4 samples decreased slightly from 29.18 to 16.07 in Fig. 4. It should be due to the disorder increase caused by the diffusion of Ti doped into Sb_2Te_3 thin films. And the optical band gap decreases from 1.32 eV to 1.25 eV. According to Burstein – Moss theory [39], the decrease in the band gap can be written as ΔE_g, which is explicitly given by the Eq. 5,

$$\Delta E_g = \frac{\left(3\pi^2 n\right)^{\frac{2}{3}}}{2m_{VC}^*} \quad , \quad (5)$$

where n refers to the carrier concentration. At a low doping concentration, it is expected that the effective mass m_{VC}^* is either basically the same or has little influence. This Eq. 4 shows that the carrier concentration is positively correlated to the size of the optical band gap. This should be due to the reduction in the number of carriers, which is caused by the Ti doping as previously mentioned in the Ti bonding analysis. It can be expected that the optical band gaps of the samples will also decrease. This is confirmed by the fitting results based on the experimental data presented in Fig. 4.

2.4 Nonlinear optical absorption and damage

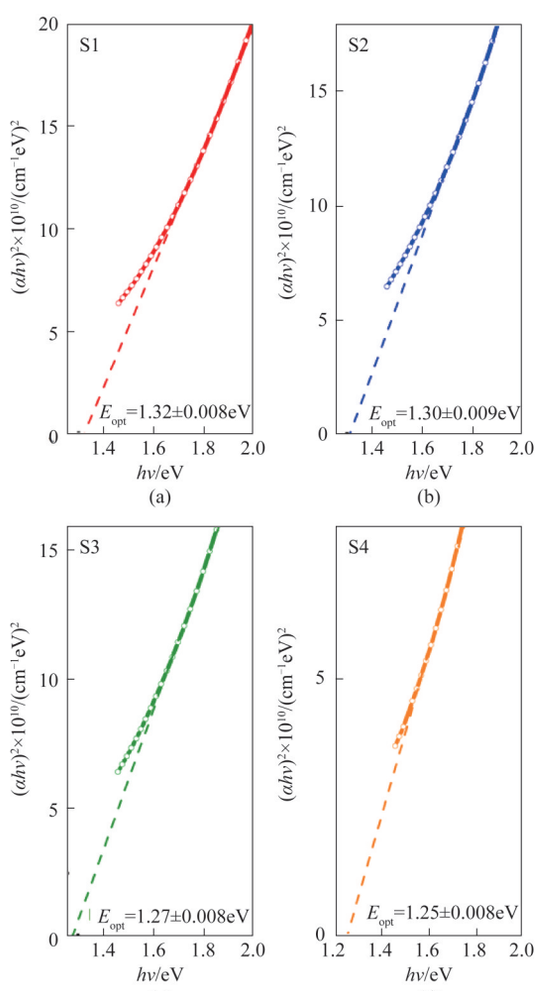

Fig. 4 The optical band gaps of the Ti-doped Sb_2Te_3 thin films (a) S1, (b) S2, (c) S3, (d) S4
图4 Ti掺杂Sb_2Te_3薄膜的光学带隙拟合曲线 (a) S1,(b) S2,(c) S3,(d) S4

threshold

A self-built open-aperture Z-scan system is employed to determine the NOA characteristics of the Ti-doped Sb_2Te_3 thin films, which is excited by an 800 nm femtosecond laser. Each sample film drives by using a stepping motor to traverse along the Z-axis at a step of 1 mm around the laser focus point. The transmitted light intensity is measured by one detector, and compared with the measuring data of another detector to obtain the normalized transmittance [3]. It is noteworthy that the experiment must be performed at a relatively low power to ensure low nonlinear scattering interference and samples damage. Furthermore, possible background nonlinear effects were excluded using the transmission measurements under the same experimental conditions including the substrates.

Figure 5 shows the NOA behavior of the S1-S4 samples, where the data points are measured from the experimental, and yields the fitted curves. It is found that the normalized transmittance first increases with an approach to the laser focus, and then gradually decreases as the measurement point moves away. Obviously, the normalized transmittance curve of each sample in Fig. 5 is positively symmetric for the measurement focus coordinates, indicating a reversible saturation absorption (SA) behavior of the sample at reasonable experimental laser intensity. This property is generated because the optical band gaps of 1.32~1.25 eV are smaller than the photon energy of the excitation laser at 800 nm wavelength (equal to 1.55 eV). Thus, the electrons in the valence band are excited by absorbing the energy of the incident photons and transition directly to the conduction band. In this case, when the light intensity is sufficiently strong, the ground state electrons become exhausted. Due to the Pauli exclusion principle, further photon absorption is prevented and a bleaching effect occurs at the position of the laser focusing on the sample film, which is also consistent with the saturated absorption theory.

In order to more specifically reflect the nonlinear absorption of the Ti-doped Sb_2Te_3 thin films, the nonlinear coefficient β, which is defined from $\alpha = \alpha_0 + \beta I$, can be estimated (based on sheik bohea's Z-scan theory) from the following Eq. 6 [40].

$$T_{OA} = \sum_{m=0}^{\infty} \frac{\left[-\dfrac{\beta I_0 L_{eff}}{\left(1+\dfrac{z^2}{{z_0}^2}\right)}\right]^m}{(m+1)^{\frac{3}{2}}} \quad , \quad (6)$$

where T_{OA} is the normalized transmittance, I_0 is the laser intensity at the focal point, z refers to the current sample position (the distance from the focal point), z_0 is dependent on the optical Rayleigh length, and L_{eff} is the effective thickness calculated from the Eq. 7 that relates to both the linear absorptivity α_0 and the physical thickness L of the films [41].

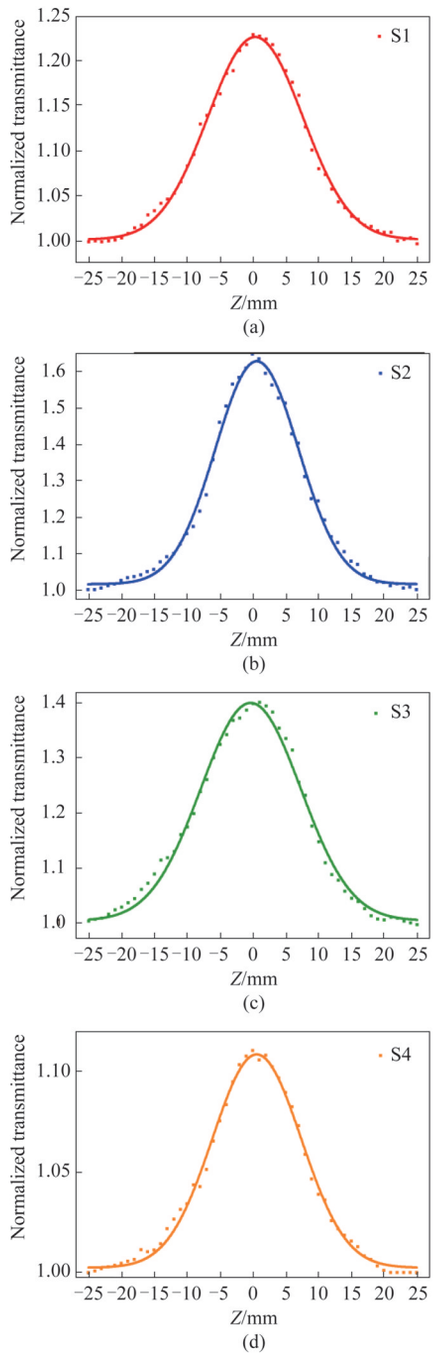

Fig. 5　The normalized transmittance curves of the Ti-doped Sb_2Te_3 thin films (a) S1, (b) S2, (c) S3, (d) S4
图 5　Ti 掺杂 Sb_2Te_3 薄膜的归一化透射率曲线 (a) S1, (b) S2, (c) S3, (d) S4

$$L_{eff} = \frac{1 - e^{-\alpha_0 L}}{\alpha_0} \quad . \quad (7)$$

In applications, great attention is often paid to both the nonlinear absorption coefficient and damage threshold of materials. Not only the nonlinear absorption coefficients were measured, but also the damage threshold in this investigation, as shown in Fig. 6 and Table 4. Interestingly, with the increase of Ti doping, the damage thresholds of Ti-doped Sb_2Te_3 films increase from 188.6

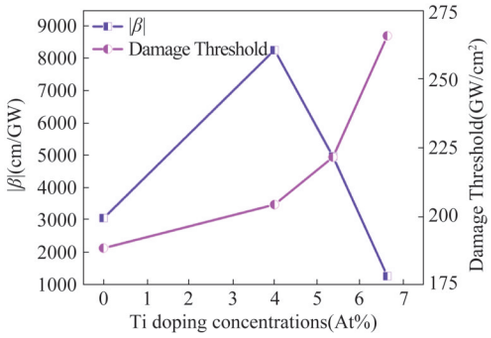

Fig. 6 Absolute value of the nonlinear absorption coefficient β and damage threshold of the Ti-doped Sb_2Te_3 thin films with different doping concentration
图6 不同Ti掺杂浓度Sb_2Te_3薄膜的非线性吸收系数β绝对值及损伤阈值大小的变化

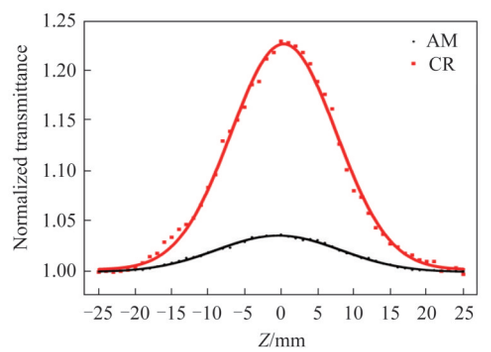

Fig. 7 Normalized transmittance curves of the amorphous and crystalline Sb_2Te_3 thin films
图7 非晶态与晶态Sb_2Te_3归一化透射率曲线对比

Table 4 Nonlinear absorption coefficient and Damage Threshold of the Ti-doped Sb_2Te_3 thin films
表4 Ti掺杂Sb_2Te_3薄膜的非线性吸收系数及损伤阈值

Sample	Ti (Atomic %)	L_{eff}/nm	β (cm/GW)	Damage Threshold (GW/cm²)
S1-AM	0	16.89	−507.4	−
S1	0	16.91	−3 044.6	188.6
S2	4.00	16.63	−8 247.5	204.4
S3	5.37	17.31	−4 952.3	221.6
S4	6.64	16.94	−1 246.6	265.5

to 265.5 GW/cm², which is advantageous for Sb_2Te_3 films that act as saturated absorbers in nonlinear devices. Notably, the damage threshold here is only a qualitative experimental result, that is, when the laser power gradually increases, the test film can no longer maintain good and reversible nonlinear absorption characteristics, it can be judged that it reaches the damage threshold.

The saturation absorption spectrum is determined only by the line width and laser intensity of the atomic energy level transition involved. Therefore, it is an effective means to regulate the optical characteristics of Sb_2Te_3 films including the optical band gap and the saturation absorption coefficient by controlling the titanium doping concentration. According to the saturation absorption theory where the electron absorbing photons lead to transition occurrence, a narrower optical band gap implies an easier absorption effect. Experimental results show that the nonlinear absorption coefficient does not keep increasing with the decrease of optical band gap in the Ti-doped Sb_2Te_3 films. Combined with the results above on the effect of titanium doping on the sample crystallinity, it is not difficult to speculate on the real reason why the crystallization is inhibited. The inhibition of crystallization will weaken the nonlinear absorption effect. In order to show that this is indeed a competitive factor, the normalized transmittance curves of the amorphous (AM) and crystalline (CR) Sb_2Te_3 is given in Fig. 7, and the other specific parameters are listed in Table 4. Obviously, the nonlinear absorption of the crystalline Sb_2Te_3 is much stronger. Therefore, the increase in Ti doping concentration reduces the optical band gap width and favors saturation absorption while inhibiting the crystallization, resulting in a competitive relationship.

3 Conclusion

In summary, this investigation confirms that the Sb_2Te_3 thin film microstructure and its optical properties can be effectively regulated by proper titanium doping, especially with its potential value as saturated absorbers in future nonlinear device applications. The Ti-doped Sb_2Te_3 film samples with different titanium doping concentrations are prepared using a magnetron sputtering tool. For the microstructure, the X-ray diffraction results indicate that the samples are crystalline with a R3m rhombohedral structure and it is determined that an increase of doping with Ti inhibits crystallization, which leads to a grain size decrease. For the optical properties, with the increase of the Ti doping concentration, the optical band gap decreases from 1.32 eV to 1.25 eV caused by the reduction in the number of carriers due to the Burstein-Moss effect. By the open-aperture Z-scan system, all the samples exhibited significant nonlinear optical properties for saturated absorption and a high damage threshold with the increase of Ti doping excited by a femtosecond laser at the wavelength of 800 nm. The study found the increase in Ti doping concentration reduces the optical band gap width and favors saturation absorption while inhibiting the crystallization, resulting in a competitive relationship. In conclusion, Ti doped Sb_2Te_3 thin films have broad potential applications in the field of nonlinear devices such as saturated absorbers.

References

[1] Chen Y H, Sun L, Zhou Y X, *et al*. Chemical understanding of resistance drift suppression in Ge-Sn-Te phase-change memory materials [J]. *J. Mater. Chem. C.*, 2020, **8**(1): 71-7.
[2] Hajijafarassar A, Martinho F, Stulen F, *et al*. Monolithic thin-film chalcogenide-silicon tandem solar cells enabled by a diffusion barrier [J]. *Sol. Energ. Mat. Sol. C.*, 2020, **207**(11): 334-44.
[3] Wang J, Jin F, Cao X R, *et al*. In_2Te_3 thin films: a promising nonlinear optical material with tunable nonlinear absorption response [J]. *Rsc. Adv.*, 2016, **6**(105): 103357-63.
[4] Yadav R K, Sharma R, Aneesh J, *et al*. Saturable absorption in one-dimensional Sb_2Se_3 nanowires in the visible to near-infrared region [J]. *Opt. Lett.*, 2016, **41**(9): 2049-52.

[5] Wang K P, Feng Y Y, Chang C X, *et al*. Broadband ultrafast nonlinear absorption and nonlinear refraction of layered molybdenum dichalcogenide semiconductors [J]. *Nanoscale*, 2014, **6**(18): 10530-5.

[6] Cirloganu C M, Padilha L A, Fishman D A, *et al*. Extremely nondegenerate two-photon absorption in direct-gap semiconductors [J]. *Opt. Express*, 2011, **19**(23): 22951-60.

[7] Liu C M, Yuan Y F, Cheng L, *et al*. Tunable nonlinear optical absorption in amorphous and crystalline Sb_2Se_3 thin films [J]. *J. Alloy Compd.*, 2019, **791**: 753-60.

[8] Verrone R N, Moisset C, Lemarchand F, *et al*. Thickness-dependent optical nonlinearities of nanometer-thick Sb_2Te_3 thin films: implications for mode-locking and super-resolved direct laser writing [J]. *Acs. Appl. Nano Mater*, 2020, **3**(8): 7963-72.

[9] Barik A R, Adarsh K V, Naik R, *et al*. Photoinduced transparency of effective three-photon absorption coefficient for femtosecond laser pulses in $Ge_{16}As_{29}Se_{55}$ thin films [J]. *Appl. Phys. Lett.*, 2011, **98**(20): 1111-20.

[10] Cheng L, Yuan Y F, Liu C M, *et al*. Linear and nonlinear optical properties modulation of Sb_2Te_3/GeTe bilayer film as a promising saturable absorber [J]. *Results Phys.*, 2019, **13**(10): 2282-9.

[11] Zhu M, Wu L C, Rao F, *et al*. The effect of titanium doping on the structure and phase change characteristics of Sb_4Te [J]. *J. Appl. Phys.*, 2013, **114**(12): 4302-11.

[12] Qiu F, Narusawa T. Ion-implanted Ti-doped chalcogenide glass waveguide as a candidate for tunable lasers [J]. *J. Opt. Soc. Am B*, 2011, **28**(6): 1490-2.

[13] Li K Q, Peng L Y, Zhu L G, *et al*. Vacancy-mediated electronic localization and phase transition in cubic Sb_2Te_3 [J]. *Mat. Sci. Semicon Proc.*, 2021, **135**(10): 6052-8.

[14] Cao X R, Meng C M, Li J, *et al*. Characterization of interfacial barrier charging as a resistive switching mechanism in Ag/Sb_2Te_3/Ag heterojunctions [J]. *Phys. Chem. Chem. Phys.*, 2018, **20**(27): 18200-6.

[15] Liu B, Song Z T, Feng S L, *et al*. Characteristics of chalcogenide nonvolatile memory nano-cell-element based on Sb_2Te_3 material [J]. *Microelectron Eng.*, 2005, **82**(2): 168-74.

[16] Wang G F, Cagin T. Electronic structure of the thermoelectric materials Bi_2Te_3 and Sb_2Te_3 from first-principles calculations [J]. *Phys. Rev. B*, 2007, **76**(7): 75201-8.

[17] Zybala R, Mars K, Mikula A, *et al*. Synthesis and Characterization of Antimony Telluride for Thermoelectric and Optoelectronic Applications [J]. *Arch Metall Mater*, 2017, **62**(2): 1067-70.

[18] George P A, Strait J, Dawlaty J, *et al*. Ultrafast optical-pump terahertz-probe spectroscopy of the carrier relaxation and recombination dynamics in epitaxial graphene [J]. *Nano Lett.*, 2008, **8**(12): 4248-51.

[19] Zhang H J, Liu C X, Qi X L, *et al*. Topological insulators in Bi_2Se_3, Bi_2Te_3 and Sb_2Te_3 with a single Dirac cone on the surface [J]. *Nat. Phys.*, 2009, **5**(6): 438-42.

[20] Liu S, Wei J S, Gan F X. Nonlinear absorption of Sb-based phase change materials due to the weakening of the resonant bond [J]. *Appl. Phys. Lett.*, 2012, **100**(11): 903-9.

[21] Jiang G B, Yi J, Miao L L, *et al*. Bismuth Telluride nanocrystal: broadband nonlinear response and its application in ultrafast photonics [J]. *Sci. Rep-Uk*, 2018, **8**: 2355-63.

[22] Ganeev R A, Popov V S, Zvyagin A I, *et al*. Exfoliated Bi_2Te_3 nanoparticle suspensions and films: morphological and nonlinear optical characterization [J]. *Nanophotonics-Berlin*, 2021, **10**(15): 3857-70.

[23] Li X L, Rao F, Song Z T, *et al*. Experimental and theoretical study of silicon-doped Sb_2Te_3 thin films: Structure and phase stability [J]. *Appl. Surf. Sci.*, 2011, **257**(10): 4566-8.

[24] Hu S W, Liu B, Li Z, *et al*. Identifying optimal dopants for Sb_2Te_3 phase-change material by high-throughput ab initio calculations with experiments [J]. *Comp. Mater Sci.*, 2019, **165**: 51-8.

[25] Drasar C, Steinhart M, Lost'ak P, *et al*. Transport coefficients of titanium-doped Sb_2Te_3 single crystals [J]. *J. Solid State Chem.*, 2005, **178**(4): 1301-7.

[26] Lostak P, Drasar C, Navratil J, *et al*. Sb_2Te_3 single crystals doped with chromium atoms [J]. *Cryst Res. Technol*, 1996, **31**(4): 403-13.

[27] Drasar C, Lostak P, Navratil J, *et al*. Optical-properties of titanium-doped Sb_2Te_3 single-crystals [J]. *Physica Status Solidi B-Basic Research*, 1995, **191**(2): 523-9.

[28] Chen L Y, Feng X W, Su Y, *et al*. Design of a scanning ellipsometer by synchronous rotation of the polarizer and analyzer [J]. *Appl. Optics*, 1994, **33**(7): 1299-305.

[29] Boguslawski J, Sobon G, Zybala R, *et al*. Investigation on pulse shaping in fiber laser hybrid mode-locked by Sb_2Te_3 saturable absorber [J]. *Opt Express*, 2015, **23**(22): 29014-23.

[30] Liu C M, Cheng L, Yuan Y F, *et al*. Contrastive investigation on linear optical properties and nonlinear absorption behaviors between Sb_2Se_3 and Sb_2Te_3 thin films [J]. *Mater Res Express*, 2019, **6**(8): 6446-55.

[31] Devesa S, Rooney A P, Graca M P, *et al*. Williamson-hall analysis in estimation of crystallite size and lattice strain in $Bi_{1.34}Fe_{0.66}Nb_{1.34}O_{6.3}$ prepared by the sol-gel method [J]. *Mater Sci. Eng. B-Adv.*, 2021, **263**(11): 4830-7.

[32] Zhang L, Song S N, Xi W, *et al*. Effect of Ti additions on structure and phase stability of Sb_2Te_3 thin films by experimental and theoretical methods [J]. *J. Mater Sci-Mater El*, 2018, **29**(6): 4704-10.

[33] Zhu M, Xia M J, Song Z T, *et al*. Understanding the crystallization behavior of as-deposited Ti-Sb-Te alloys through real-time radial distribution functions [J]. *Nanoscale*, 2015, **7**(21): 9935-44.

[34] Vainshtein B K, Fridkin V M, Indenbom V L. Principles of formation of the atomic structure of crystals [J]. *Modern Crystal*, 2000, **1**: 1-123.

[35] Kulbachinskii V A, Miura N, Nakagawa H, *et al*. Influence of Ti doping on galvanomagnetic properties and valence band energy spectrum of $Sb_{2-x}Ti_xTe_3$ single crystals [J]. *J. Phys-Condens Mat.*, 1999, **11**(27): 5273-82.

[36] Tauc J, Grigorov R, Vancu A. Optical properties and electronic structure of amorphous germanium [J]. *J. Phys. Soc. Jpn.*, 1966, **21**: 123-33.

[37] Priyadarshini P, Das S, Alagarasan D, *et al*. The impact of fluence dependent proton ion irradiation on the structural and optical properties of $Bi_5In_{30}Se_{65}$ thin films for nonlinear optical devices [J]. *Rsc. Adv.*, 2022, **12**(8): 5012-26.

[38] Carey J J, Allen J P, Scanlon D O, *et al*. The electronic structure of the antimony chalcogenide series: Prospects for optoelectronic applications [J]. *J. Solid State Chem.*, 2014, **213**: 116-25.

[39] Yuan Y F, Liu C M, Su J, *et al*. Structural and optical properties of Ti-doped InTe thin films [J]. *J. Phys. Chem. C*, 2018, **122**(11): 6267-72.

[40] Sheikbahae M, Said A A, Wei T H, *et al*. Sensitive measurement of optical nonlinearities using a single beam [J]. *IEEE J. Quantum Elect.*, 1990, **26**(4): 760-9.

[41] Zhang R F, Guo D Z, Zhang G M. Strong saturable absorption of black titanium oxide nanoparticle films [J]. *Appl. Surf. Sci.*, 2017, **426**: 763-9.